scientific reports

Check for updates

OPEN

Numerical investigation of soil-tunnel interaction under surface blast loads with regression-based energy correlations

Abdullah H. Alsabhan[1], Ibraheem Rais[2], Junaid Ahemad Khan[2], Aklilu Shitu Gebremariam[3]✉, Md. Rehan Sadique[2], Shamshad Alam[1] & Jibran Qadri[4]

Growing emphasis on sustainable urban development has intensified the use of underground urban space for transport and protection. During war or terrorism, underground tunnels can function as protective structures, so accurately assessing their response to surface blasts is essential. This study presents a three-dimensional numerical investigation of a circular metro tunnel embedded in sandy clay and subjected to surface detonation. The soil is modelled with Mohr–Coulomb plasticity, while the tunnel lining and reinforcement adopt concrete damaged plasticity and Johnson–Cook models. Blast pressures are applied via the CONWEP formulation (TM 5-855-1), and the simulation captures coupled interactions between soil, lining, reinforcement and blast wave. The framework is validated against analytical peak overpressure predictions, empirical crater dimensions and experiments on blast-loaded reinforced concrete slabs, showing acceptable deviations. Crater-size formulas are recalibrated for sandy clay using simulations with 25–1000 kg TNT, improving agreement within this range. An energy-based framework relates TNT weight to kinetic, plastic dissipation and strain energy in soil, providing meaningful insight into blast energy transmission, absorption and dissipation. The effect of charge magnitude on soil stress, liner deformation and tensile damage is assessed for overburden depths of 15, 12 and 9 m; shallow tunnels suffer greater deformation and damage under increasing blast intensity. Performance criteria identify safe and unsafe burial depths for different charges. Regression-based energy and deformation relationships enable quantitative comparisons of tunnel responses within the defined scope and assumptions.

Keywords Clayey soil, Finite element method, Surface blasting, Tunnel lining, Soil-tunnel interaction, Tension damage

The use of underground spaces for road and transportation infrastructure is essential for modern urban growth and sustainable development. Underground structures such as tunnels play a vital role in easing traffic congestion, protecting utilities, and supporting drainage and metro systems in densely populated areas[1–4]. However, the changing global security landscape marked by rising incidents of terrorism and geopolitical conflicts has raised concerns over the vulnerability of critical infrastructures, including underground tunnels. Explosive attacks, including those involving conventional bombs, missiles, and drones, have been increasingly reported in recent decades, posing serious threats to civilian life and urban stability[5]. Figure 1 illustrates various forms of terrorist attacks, showing that explosive events are among the most prevalent[6]. Consequently, there is a growing need to evaluate and improve the blast resistance of underground structures such as tunnels, bunkers, and shelters that may serve protective functions during warfare or terrorist events.

Underground tunnels, originally constructed for transportation and utility purposes, must now also withstand surface explosions. These threats may occur unexpectedly and bypass traditional protective or mitigation systems, especially if the explosion originates on the ground surface. While the risk from internal tunnel explosions can be reduced through strict security, access control, and the integration of active mitigation

[1]Department of Civil Engineering, College of Engineering, King Saud University, Riyadh, Saudi Arabia. [2]Department of Civil Engineering, Zakir Hussain College of Engineering and Technology, Aligarh Muslim University, Aligarh 202002, India. [3]Addis Ababa Science and Technology University, Akaki-Kality, Addis Ababa, Ethiopia. [4]Department of Geotechnical Engineering, College of Civil, Environmental and Architectural Engineering Sciences, University of Padova, Via Marzolo, Padova, Italy. ✉email: aklilu.shitu@aastu.edu.et

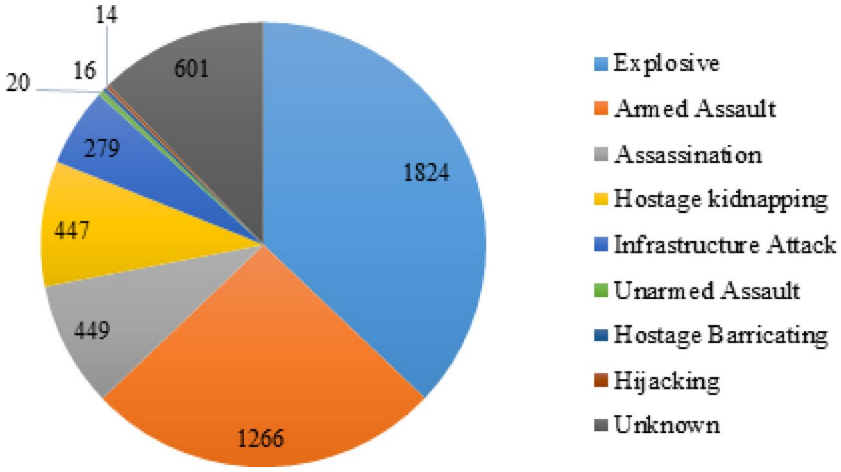

Fig. 1. Terrorist attacks employing various methods worldwide in 2021[6].

systems[7,8], surface blasts present a unique challenge due to their direct interaction with soil layers and the potential transmission of shock waves toward buried structures. Hence, it becomes imperative to understand the response mechanisms of underground tunnels subjected to surface blast loading.

Blast loads differ significantly from static or seismic loads in terms of their magnitude, duration, and strain rate effects. The interaction between blast waves and the surrounding soil-structure system is highly nonlinear and transient[9,10]. Despite its importance, experimental analysis of buried structures under blast loads remains limited due to various practical constraints. These include high costs, safety regulations, and the logistical complexity of setting up controlled explosions involving soil or rock masses[11–13]. For example, De et al.[14] conducted both experimental and numerical investigations of tunnel liners protected by geofoam against surface blasts and demonstrated that geofoam effectively reduced the transmission of stress and pressure to the lining, thus enhancing safety. However, such experimental approaches remain rare, prompting researchers to turn toward advanced numerical simulations.

In recent years, advancements in computational methods and the increasing availability of high-performance computing resources have encouraged the development of robust numerical tools based on the finite element method (FEM). These methods provide a cost-effective, safe, and flexible way to simulate and study soil-structure interaction under extreme loading scenarios such as surface blasts[13–16]. FEM-based tools allow the integration of complex constitutive models for soil and structural materials, accurate modeling of blast wave propagation, and observation of stress–strain responses in the tunnel components.

Several notable studies have demonstrated the effectiveness of numerical modeling for tunnel blast analysis. For instance, Mandal et al.[17] performed numerical simulations of shallow tunnels buried in soil and subjected to surface blasts. Their findings suggested that a tunnel with a 300 mm thick liner remained safe under a 500 kg trinitro toluene (TNT) explosion when buried at a depth of 8 m. Similarly, Rashiddel et al.[18] analyzed the influence of different longitudinal joint shapes in tunnel liners and concluded that curved joints were more effective in mitigating blast-induced damage. These studies underscore the importance of material choice, tunnel geometry, and burial depth in determining a structure's blast resistance.

One of the widely accepted numerical approaches for modeling blast loading is the CONWEP (Conventional Weapons Effects) model, based on the US Department of Army technical manual TM 5-855-1[19]. This model, integrated into platforms like Abaqus, estimates pressure–time histories of blast loads and has been frequently used in past research to simulate the effects of surface explosions on underground structures[20–22]. Despite its empirical nature, CONWEP remains popular due to its simplicity, accuracy, and practical applicability for engineering design.

However, despite the extensive use of numerical modeling, most existing studies have primarily focused on tunnels embedded in rock masses, while limited attention has been given to tunnels surrounded by soil, especially soft or intermediate soil types. Among these, sandy clay, a commonly encountered soil in urban tunneling projects, has not been thoroughly investigated under surface blast loading conditions. Furthermore, the dynamic behavior of tunnels in sandy clay under such loading, including the transfer and dissipation of energy, remains insufficiently explored in the literature.

To address these gaps, the present study conducts a comprehensive numerical investigation using finite element simulations to analyze the behavior of a metro tunnel constructed in sandy clay subjected to surface blast loads. The simulation approach incorporates advanced constitutive models to represent soil (Mohr–Coulomb), concrete (Concrete Damaged Plasticity), and steel reinforcement (Johnson–Cook plasticity), with the blast load applied using the CONWEP method. Validation of the simulation process was carried out through comparisons with peak pressure predictions from TM 5-855-1[19] and empirical crater diameter correlations established by Ambrosini et al.[23]. Although empirical crater-size relationships such as those by Ambrosini et al. provide useful first-order estimates, their applicability is often limited by soil type and charge range. This study refines these formulations by recalibrating crater diameter and apparent depth using three-dimensional simulations for sandy clay. In contrast to previous tunnel blast studies focused mainly on deformation or damage, the present

work introduces an energy-based framework by correlating kinetic, plastic dissipation, and strain energies with explosive charge. These regression-based relationships offer simplified tools for preliminary design, rapid vulnerability assessment, and comparative evaluation of burial depth and blast intensity for underground tunnels and protective structures. The study further evaluates safety levels and potential damage at various overburden depths (15 m, 12 m, and 9 m) for a range of TNT charge magnitudes. In addition, stresses in the surrounding soil, tunnel liner deformations, and tensile damage patterns are assessed to quantify the structural vulnerability under varying blast intensities.

Numerical modelling

Finite element (FE) modeling of soil and reinforced concrete liner

The numerical model comprises a soil domain containing a circular tunnel liner with an internal diameter of 5 m and a wall thickness of 0.35 m. The overall domain dimensions are 40 m × 40 m in cross-section and 30 m in length. Figure 2 presents the components of the numerical model. The tunnel liner is constructed using Reinforced Cement Concrete (RCC), incorporating both internal and external steel reinforcement grids. In the longitudinal direction, 10 mm diameter steel bars are placed at 850 mm center-to-center spacing, while in the circular direction, 12 mm bars are spaced at 250 mm center-to-center as shown in Fig. 2c.

The finite element mesh employed for the surface blast analysis is illustrated in Fig. 3. Both the tunnel liner and soil models have been meshed using a C3D8R element, an 8-noded linear brick with reduced integration

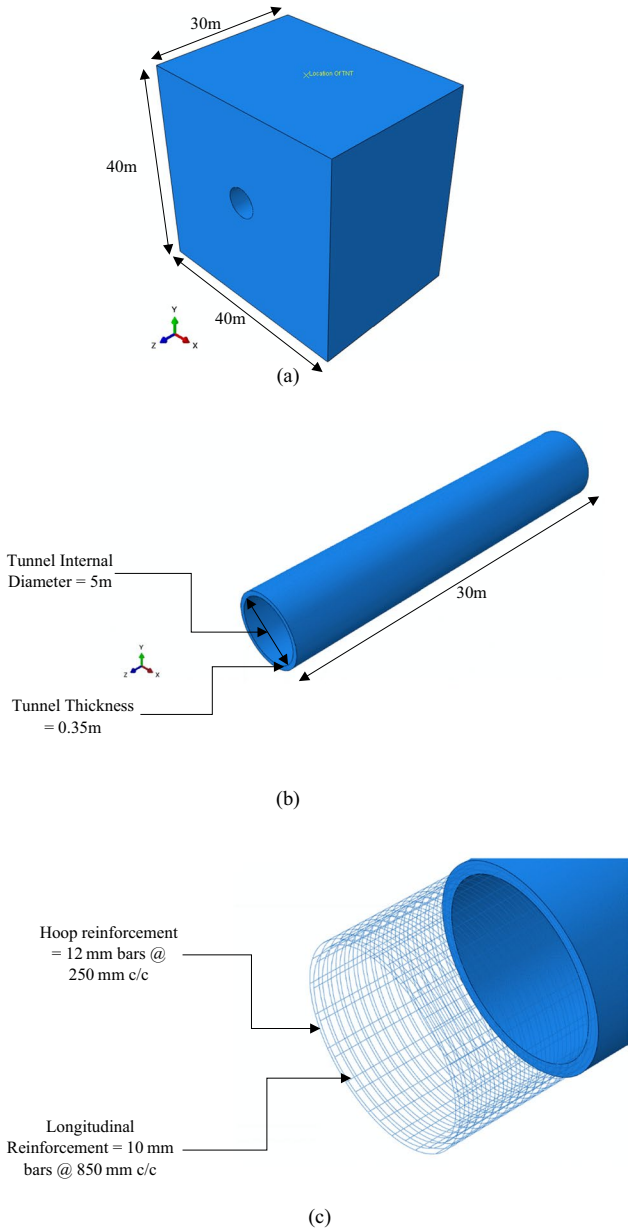

Fig. 2. Geometry of soil-tunnel model (**a**) Soil model (**b**) Tunnel liner (**c**) Steel reinforcement.

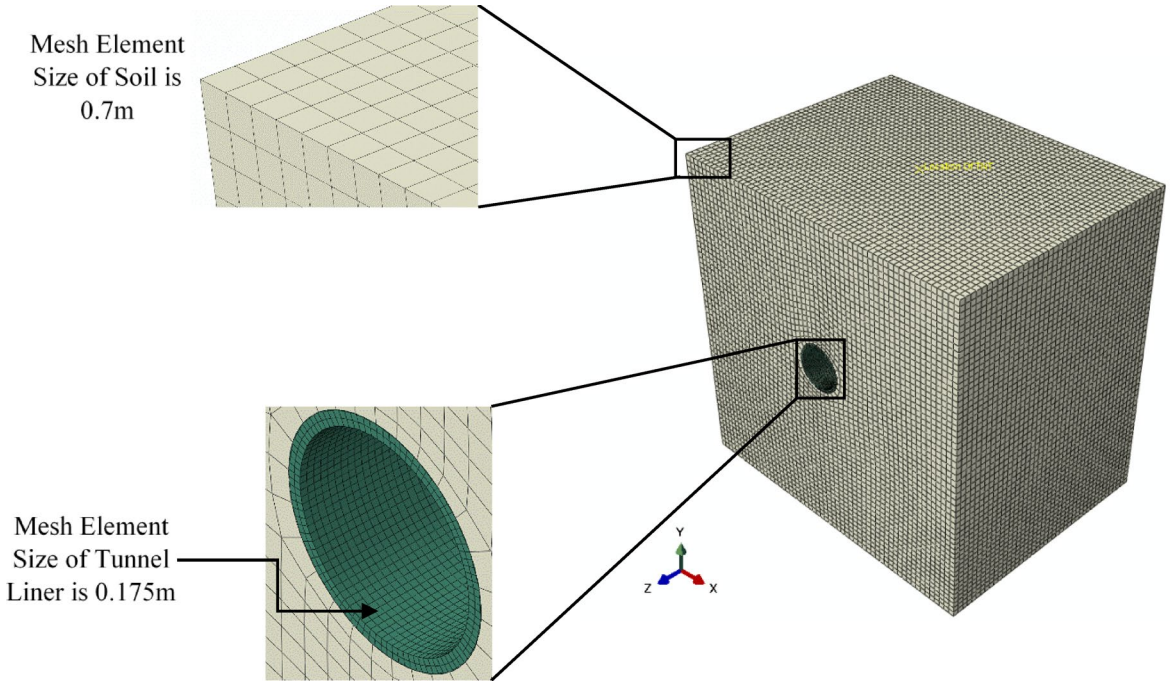

Fig. 3. Meshing details of different parts of the model.

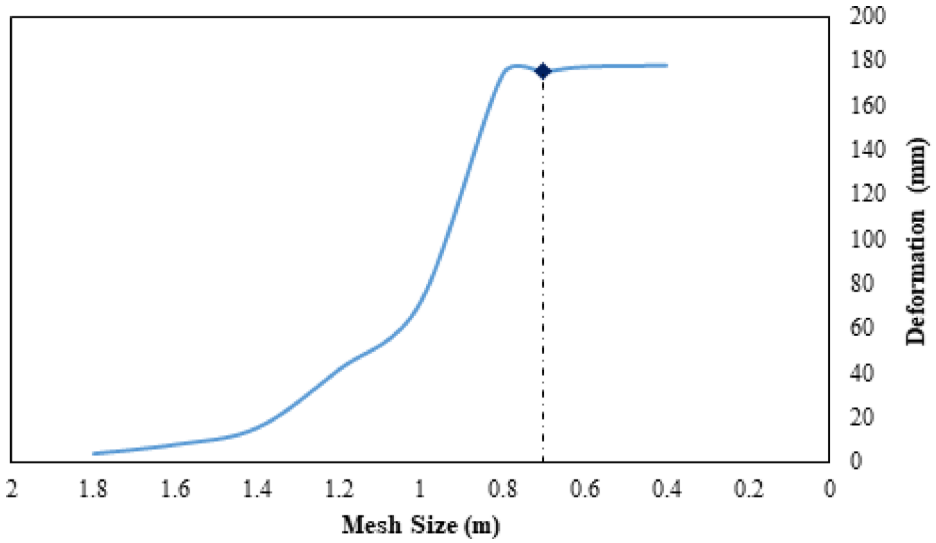

Fig. 4. A mesh convergence study was conducted to determine an appropriate soil element size.

and hourglass control. The element size for the tunnel liner is set to 0.175 m, while for the soil, it is 0.7 m, based on the results of the mesh convergence study presented in Fig. 4. The reinforcement bars have been meshed using a B31 element, a 2-noded beam type element.

In this study, the tunnel lining is modeled along with the surrounding soil to accurately capture soil–tunnel interaction under blast-induced dynamic loading. The interaction between the soil and tunnel liner is defined using a surface-to-surface contact model. In the normal direction, a hard contact condition is applied, ensuring no penetration between the surfaces. In the tangential direction, a penalty-based friction model is implemented, where the shear resistance is governed by the soil's friction angle and the corresponding wall friction angle.

To replicate the actual field conditions, the model has been assigned the required boundary constraint against each face and dimension. The model base is fully constrained in translation and rotation ($U_x = U_y = U_z = U_{rx} = U_{ry} = U_{rz} = 0$). On the right and left lateral boundaries (blue), displacement in the y- and z- directions is permitted while U_x, U_{ry}, and U_{rz} are fixed ($U_x = U_{ry} = U_{rz} = 0$). On the front and

back boundaries (grey), displacement in the x- and y-directions is permitted while U_z, U_{rx}, and U_{ry} are fixed ($U_z = U_{rx} = U_{ry} = 0$), as shown in Fig. 5[24].

Material modeling

Soil

The soil has been modeled using Mohr–Coulomb plasticity (M-C) for this analysis. This M-C model was defined by:

$$\tau = c + \sigma tan\varphi \tag{1}$$

where,τ represents the shear stress of the soil. φ and c are the shear parameters of soil are known as the angle of internal friction and cohesion, respectively. σ stands for normal stress. The three stress invariants for a general stress state in the Mohr–Coulomb model are defined as:

$$F = R_{mc}q - ptan\varnothing - c = 0 \tag{2}$$

where,

$$R_{mc}\left(\theta, \varnothing\right) = \frac{1}{\sqrt{3}cos\varnothing} sin\left(\theta + \frac{\pi}{3}\right) + \frac{1}{3}cos\left(\theta + \frac{\pi}{3}\right) tan\varnothing \tag{3}$$

$$cos\left(3\theta\right) = \left(\frac{r}{q}\right)^3 \tag{4}$$

$$p = -\frac{1}{3}trace(\sigma) \tag{5}$$

$$q = \sqrt{\frac{3}{2}(S:S)} \tag{6}$$

$$r = \left(\frac{9}{2}S * S:S\right)^{\frac{1}{3}} \tag{7}$$

$$S = \sigma + pI \tag{8}$$

Here, c denotes soil cohesion; $\varnothing$ is the deviatoric (polar) angle; and p, q, and r represent the mean (pressure) stress, the von Mises equivalent stress, and the third invariant of the deviatoric stress, respectively. S denotes the deviatoric stress.

The sandy clay properties used in this study are representative of medium-stiff deposits commonly encountered in urban metro tunnel projects and are consistent with values reported in previous tunnel–soil interaction studies. These parameters are therefore considered appropriate for capturing the global response

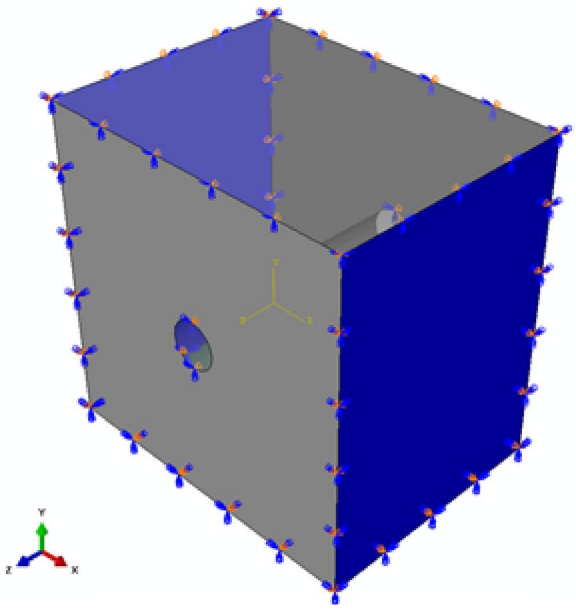

Fig. 5. Boundary conditions of the soil-tunnel model.

Soil type	Unit weight	Cohesion	Friction angle	Modulus of elasticity
Sandy clay	17.71 kN/m^3	92 kN/m^2	23°	16.8 MPa

Table 1. Properties of the soils considered in the present study[25,26].

Yield stress (kPa)	Plastic strain
92	0
210	0.015
330	0.065
360	0.12

Table 2. Soil hardening properties[25,26].

of tunnels embedded in sandy clay under surface blast loading. Material properties for the sandy clay soil were adopted from the literature[25,26] and are summarized in Tables 1 and 2.

The Mohr–Coulomb (M–C) model represents a simplified description of soil behavior under high strain-rate blast loading. Experimental studies have shown that strain-rate effects, confinement, and pore-fluid interactions can influence soil stiffness and strength; however, advanced rate-dependent constitutive models require extensive high strain-rate calibration data, which are generally unavailable for sandy clay soils. Therefore, the M–C model is adopted in this study as an engineering approximation to capture the dominant features of stress transmission and deformation in the soil–tunnel system.

Concrete

The concrete tunnel exhibits damage coupled with elasto-plasticity behavior, modeled using the concrete damaged plasticity (CDP) model. The stress (σ) and strain ($\in$) relationship for the concrete model is represented as follows:

$$\sigma_t = (1 - d_t)\, E_0(\in_t - \in_t{}^{-pl}) \tag{9}$$

$$\sigma_c = (1 - d_c)\, E_0(\in_c - \in_c{}^{-pl}) \tag{10}$$

In the Concrete Damaged Plasticity (CDP) model, t and c denote tension and compression, $\in^{-pl}$ is the plastic strain, d is the scalar damage variable, and E_0 is the initial (undamaged) elastic modulus. The CDP yield function follows the formulation of Lubliner et al. [27] and Lee & Fenves [28]:

$$F = \left(\sqrt{\frac{3\sqrt{s:s}}{2}}\right) - 3\alpha\overline{p} + \beta\hat{\overline{\sigma}}_{max} - \gamma\hat{\overline{\sigma}}_{max} - (1-\alpha)\overline{\sigma}_c \tag{11}$$

where $\hat{\overline{\sigma}}_{max}$ stands for maximum principal effective stress, $\overline{s}$ is deviatoric stress tensor.

where,

$$\alpha = \frac{\left(\frac{\sigma_{bo}}{\sigma_{c0}}\right) - 1}{2\left(\frac{\sigma_{bo}}{\sigma_{c0}}\right) - 1} \tag{12}$$

$$\beta = \frac{\widetilde{\sigma}_c}{\widetilde{\sigma}_t}(1-\alpha) - (1+\alpha) \tag{13}$$

$$\gamma = \frac{3(1-k_c)}{2k_c - 1} \tag{14}$$

$$\widetilde{\sigma}_c = \frac{\sigma_c}{1-d_t} \tag{15}$$

$$\widetilde{\sigma}_t = \frac{\sigma_t}{1-d_t} \tag{16}$$

The ratio $\frac{\sigma_{bo}}{\sigma_{c0}}$ is defined as the initial equi-biaxial compressive yield stress divided by the initial uniaxial compressive yield stress; d_t is the tensile damage variable; and k_c is the ratio of the second deviatoric stress invariant on the tensile meridian to that on the compressive meridian at initial crushing.

The concrete lining is modeled as M30-grade reinforced concrete, which is widely used in metro tunnel linings and underground infrastructure. The adopted elastic and damage parameters are consistent with published experimental and numerical studies on M30 concrete and are representative of commonly used tunnel lining materials. The CDP parameters for M30 grade concrete are provided in Table 3, along with the

Properties	Values
Density of concrete	2500 kg/m^3
Young's modulus	26.6 GPa
Poisson's ratio	0.2
Dilation angle	31°
Eccentricity	0.1
fb_0/fc_0	1.16
k	0.67
Viscosity parameter	0

Table 3. Input CDP parameters of M30 grade concrete[29].

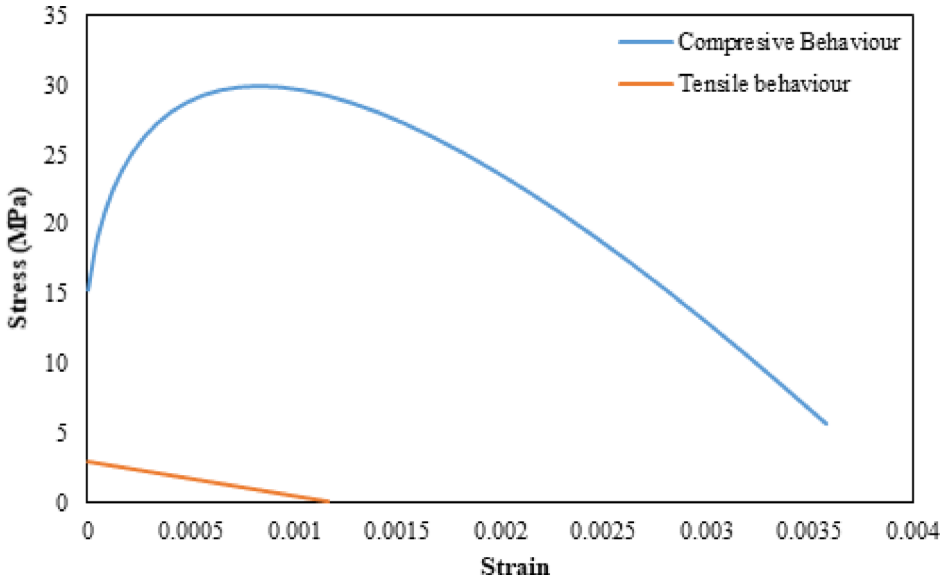

Fig. 6. Compressive and Tensile Behavior of M30 grade Concrete.

stress–strain behavior under compression and tension shown in Fig. 6, and the compression and tension damage behavior presented in Fig. 7[29].

Steel

The yield stress of the elasto-viscoplastic material for the reinforcement of the tunnel liner has been represented using the Johnson–Cook model[30], which incorporates hardening law and rate dependence. The yield stress is expressed as:

$$\sigma^o = (A + B(\in^p)^n)\left(1 + Cln\frac{\dot{\in}^p}{\dot{\in}_0}\right)\left(1 - \hat{\theta}^m\right) \tag{17}$$

where, $\dot{\in}^p$ represents equivalent plastic strain rate and $\dot{\in}_0 = {}^1/_s$ stands for reference strain rate,$\hat{\theta}$ stands for homologous temperature. A, B, C, m, and n are the model parameters.

The strain rate at the fracture point is implicitly dependent on material constants, and a non-dimensional plastic strain rate, $\in^p$, is defined as:

$$\in^p = \left[b_1 + b_2 exp\left(b_3\frac{p\prime}{q\prime}\right)\right]\left[1 + b_4 ln\left(\frac{\dot{\in}^p}{\dot{\in}_0}\right)\right](1 + b_5\hat{\theta}) \tag{18}$$

In the expression above (Eq. 18), b_1, b_2, b_3, b_4, and b_5 are material-specific empirical constants that appear in the strain-rate/fracture relation used for the steel damage formulation. The symbol p' denotes the hydrostatic (mean) effective stress (units: kPa), and q' denotes the von Mises equivalent (deviatoric) stress (units: kPa). The non-dimensional plastic strain rate is defined as $\dot{\in}_p^* = \dot{\in}^p/\dot{\in}_0$, where $\dot{\in}^p$ is the equivalent plastic strain rate (s^{-1}) and $\dot{\in}_0$ is the reference strain rate (s^{-1}).

The tunnel liner reinforcement is modeled using the Johnson–Cook constitutive model to capture strain hardening and strain-rate effects under blast loading. The adopted material parameters correspond to Fe 415

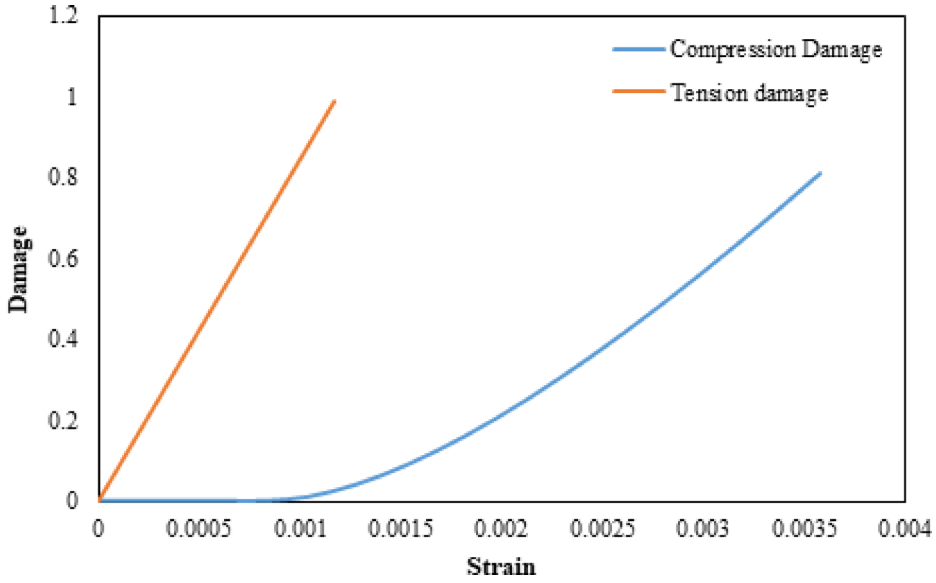

Fig. 7. Concrete compression and tension damage of M30 grade Concrete.

grade reinforcing steel, which is widely used in reinforced concrete metro tunnel linings and is characterized by a nominal yield strength of approximately 415 MPa and moderate strain-hardening behavior. In the Johnson–Cook constitutive model, the steel reinforcement is characterized by a density of 7850 kg/m^3, a Young's modulus of elasticity of 210 GPa, and a Poisson's ratio of 0.3. The adopted material constants are $b_1 = 0.07041, b_2 = 1.7312$, $b_3 = 0.551, b_4 = -0.0151$, and $b_5 = 0.00$, which correspond to high-strength reinforcing steel commonly used in reinforced concrete tunnel linings. Thermal effects are represented using a transition temperature of 273 K, a melting temperature of 1800 K, and a thermal softening exponent of 0.94. The displacement at failure is assumed to be 0.1 m, while the mechanical response is further characterized by a static yield strength of 490 MPa, a strain-hardening constant of 807 MPa, and a strain-hardening exponent of 0.73. All material parameters were adopted from published literature[31].

Explosives

Surface blasts using TNT are modeled with the CONWEP formulation over an analysis duration of 0.1 s. This methodology, commonly employed for surface-blast loading [19–21] and documented in the Abaqus manual [32], is based on the correlations of Kingery and Bulmash [33] together with experimental data reported in U.S. Army TM 5–855-1[19]. Given a user-specified TNT-equivalent mass, CONWEP evaluates the total overpressure as a function of incidence angle and time, as defined in Eqs. (19) and (20).

$$for, cos\alpha \geq 0 P(T) = P_{ind}(T)\left[1 + cos\alpha - 2cos^2\alpha\right] + P_{ref}(T)\, cos^2\alpha for, cos\alpha < 0 \tag{19}$$

$$P(T) = P_{incident} \tag{20}$$

where, $P(\mathrm{T})$ stands for the total pressure of the blast wave, $P_{ind}(T)$ stands for incident pressure, $P_{ref}(T)$ represents reflected pressure and α is the angle of incidence. The weight of TNT taken up to 1000 kg has been considered for this study.

Validation

The validation of the finite element model is presented in this section to ensure the reliability of the numerical analysis. A surface detonation transfers energy into the ground, producing three principal effects: crater formation, ground shock, and subsurface settlement. Validation in this study was performed by comparing simulated crater dimensions and ground shock responses against established empirical relations and analytical solutions. Apart from that, validation has been done by comparing the experimental result of blast load from existing literature. This comparison ensures the model's capability to accurately capture the physical behavior of soil-tunnel systems subjected to blast loading.

Validation based on peak pressure

The explosion on the surface of the soil results in ground shock, which is calculated in terms of peak pressure. The peak pressure of soil produced in surface blasting is estimated by an empirical equation specified in Technical Manual TM 5-855-1[19]. The peak pressure generated is calculated from the given equation:

$$P_o = 0.407 f p_c \left(\frac{R}{W^{1/3}}\right)^{-n} \tag{21}$$

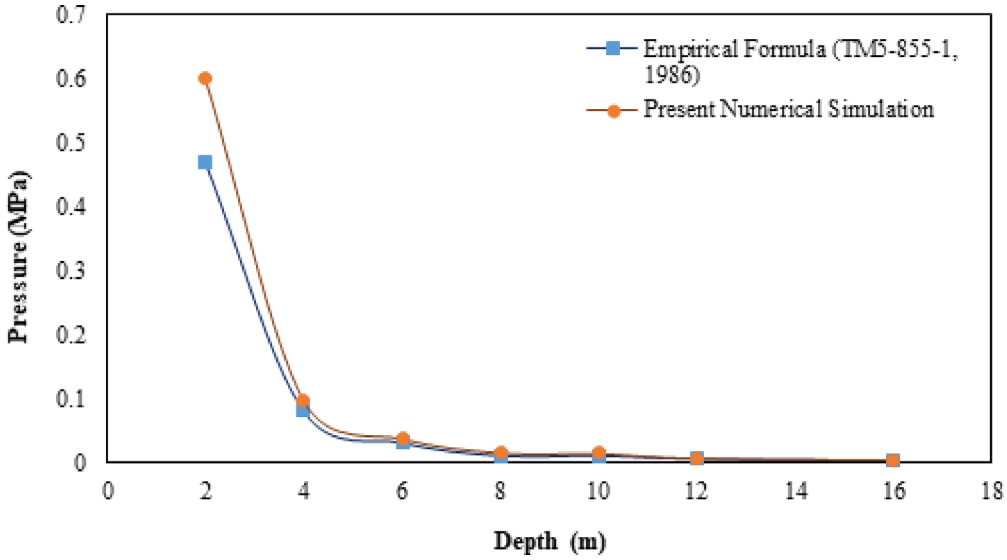

Fig. 8. Validation based on Peak Pressure[19].

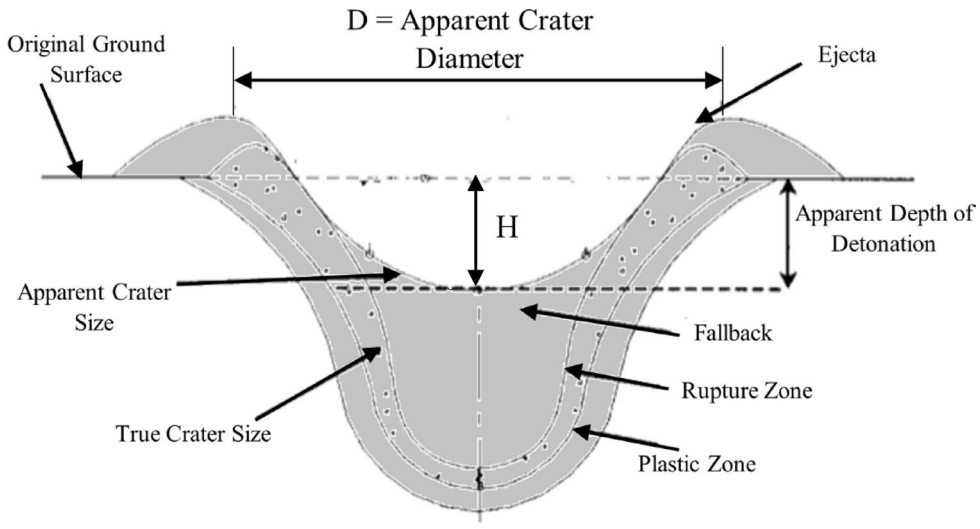

Fig. 9. Crater formation and its dimension are described by Kinney and Graham[34].

where P_o stands for peak pressure (Pascal), p_c is the acoustic impedance (for sandy clay: 44 psi/fps), coupling factor $(f) = 0.14$, R (m) is the distance from the explosive, W represent explosive weight (kg), and coefficient of attenuation $(n) = 2.5$. Figure 8 illustrates the comparison between peak pressures obtained from the empirical equation and those produced in the numerical simulation. A similar pattern is observed, with only minor differences between the two.

Validation Based on Crater Size

Upon detonation, the blast wave crushes and compacts near-surface soil, forming a crater whose size depends on the TNT charge and soil properties (e.g., void ratio, density, compressive strength, and mineralogy). Crater dimensions following Kinney and Graham[34] are presented in Fig. 9. Using approximately 200 surface-blast tests compiled by Kinney and Graham[34], Ambrosini et al.[23] proposed empirical expressions for the apparent crater diameter D and depth H. The diameter predicted by this relation is compared with the numerical results. The equations are expressed as:

$$D = 0.46W^{\frac{1}{3}} \tag{22}$$

$$H = \frac{D}{5.78} \tag{23}$$

Weight of TNT (kg)	Size of the crater (D_r) from numerical results	Size of the crater (D_r) from empirical results[23]	Percentage difference (%)
100	2.08	2.13	2.35
200	2.64	2.69	1.86
300	3.06	3.08	0.65
400	3.19	3.39	5.90
500	3.55	3.65	2.74
700	3.65	4.08	10.54
1000	4.32	4.60	6.09
Minimum relative error (%)			0.65
Maximum relative error (%)			10.54
Mean relative error (%)			4.30
Maximum absolute deviation (m)			0.43
RMSE (m)			0.213

Table 4. Comparison of the numerical and empirical crater size.

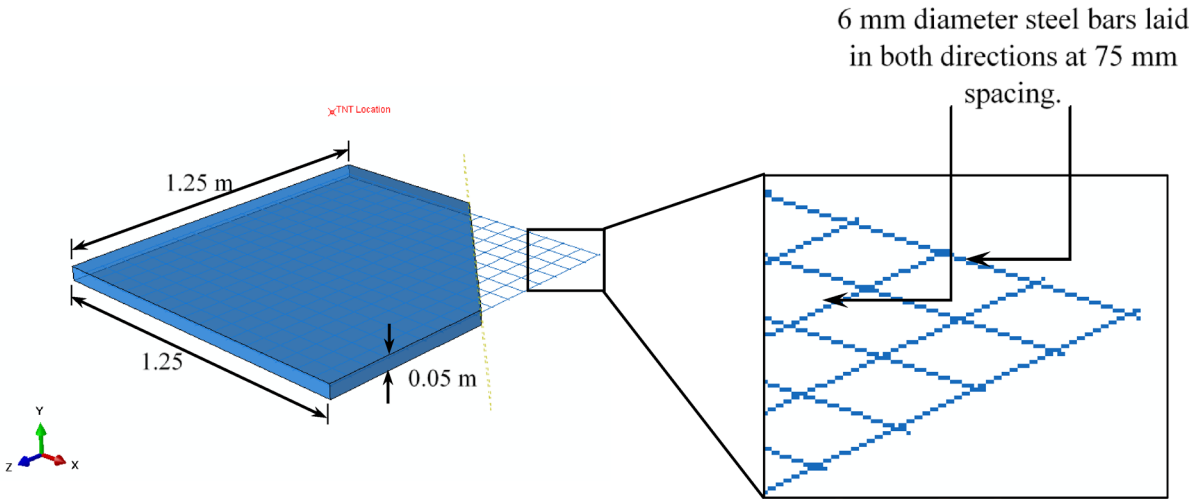

Fig. 10. Details of RC slab during experiment for numerical modelling[35].

In these expressions, W is the TNT mass (kg); D is the apparent crater diameter, which scales with $W^{\frac{1}{3}}$; and H is the apparent crater depth.

The three-dimensional domain ($40 \times 40 \times 30$ m) with sandy clay soil was discretized with a nominal mesh size of 0.7 m. For multiple TNT charges, crater diameters from the simulations were measured and averaged, then compared with values from Eq. (22)[23] (Table 4).

The relative error, calculated as the absolute difference between numerical and empirical crater diameters normalized by the empirical value, ranges from 0.65% to 10.54%, with a mean relative error of 4.30%, indicating good overall agreement. The maximum absolute deviation between numerical and empirical results is 0.43 m, observed for a TNT charge of 700 kg. Furthermore, the root-mean-square error (RMSE) across all investigated cases is 0.213 m, demonstrating that the numerical framework reproduces crater dimensions with acceptable accuracy over a wide range of explosive charge weights.

Validation Based on Experimental Results

To further validate the numerical model, a reinforced-concrete (RC) slab experiment reported in the literature was used for benchmarking. A ($1.25 \times 1.25 \times 0.05$) m slab was modelled using the CDP formulation for concrete, while reinforcement properties were adopted from prior work[35]. The slab geometry and rebar detailing are shown schematically in Fig. 10. Two charge weights—0.64 kg and 0.94 kg TNT—were applied at a standoff of 0.5 m from the slab centre[35].

The simulations reproduced damage on both faces of the slab, with more severe distress on the bottom face due to the reflection of tensile waves. For the 0.64 kg TNT charge, the numerical damage pattern closely matches the experimental observations, as shown in Fig. 11. Similarly, for the 0.94 kg TNT charge, the predicted cracking and scabbing behavior are consistent with the reported experimental results, as illustrated in Fig. 12. The close match between predictions and test results indicates that the finite element model captures the blast-induced behaviour of RC slabs with good fidelity, supporting its use for the tunnel blast-response analyses in the present study. Figure 13 presents a bar graph comparing the central deformation of the RC slab obtained from

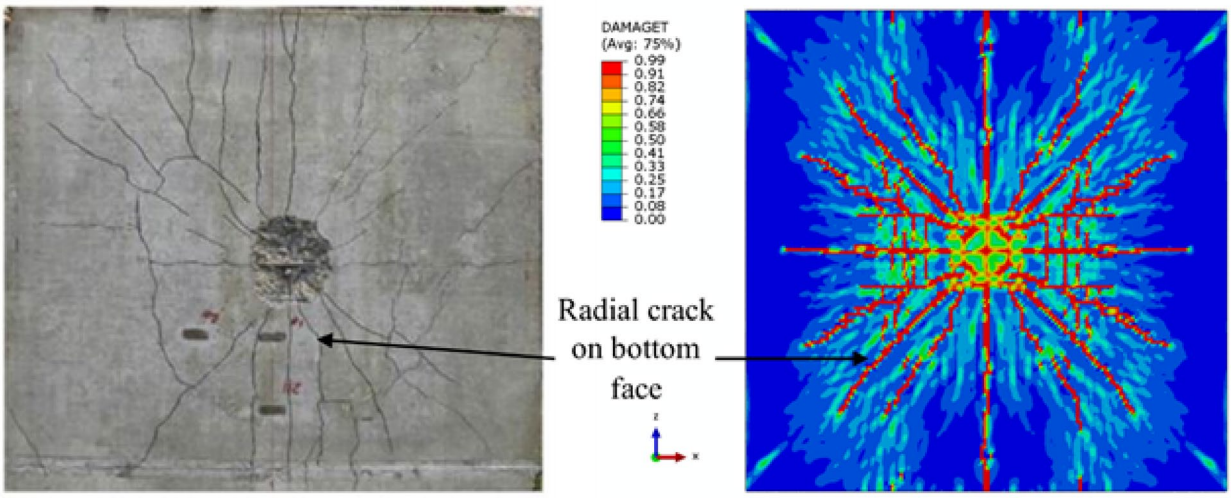

Fig. 11. Comparison of experiment and numerical results of the 0.64 kg TNT charge weight causing damage to an RC slab on bottom face.

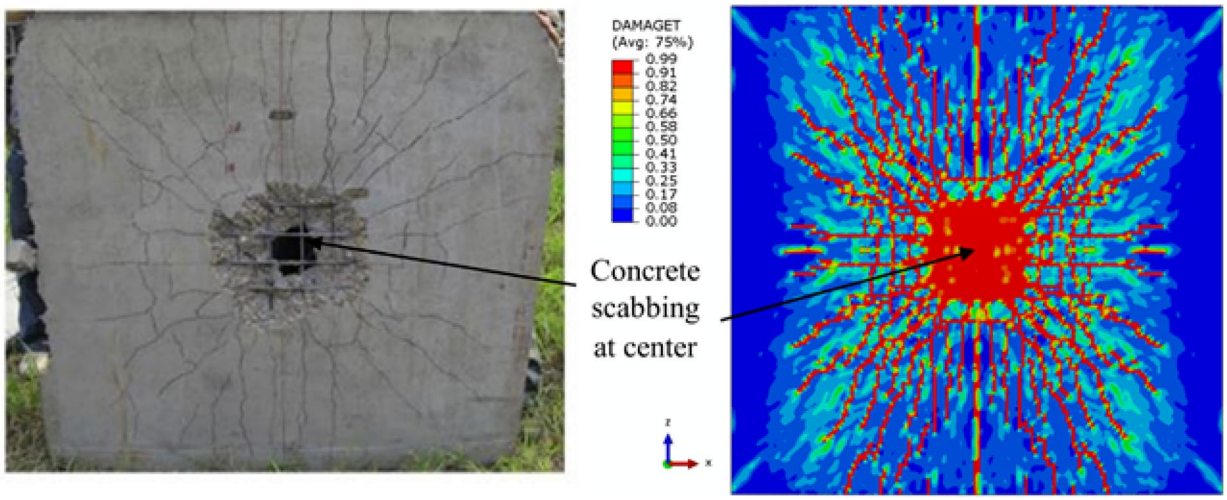

Fig. 12. Comparison of experiment and numerical results of the 0.94 kg TNT charge weight causing damage to an RC slab on bottom face.

the experiment and the numerical model for both TNT charge levels. The numerical predictions show good agreement with the experimental measurements, with only minor deviations attributed to material variability and the simplifying assumptions inherent to numerical modelling.

Results and discussion

The nonlinear response of a soil embedded tunnel subjected to surface explosions was analyzed using Abaqus/Explicit. The assessment focused on blast-induced energy, ground settlement, and damage to the tunnel lining for varying TNT weights. In addition, three cross sections of the soil tunnel with overburden depths of 15 m, 12 m, and 9 m have been analyzed for different weights of TNT.

Regression forms, parameter meaning, and applicability

The regression relationships proposed in this study are presented in the same functional forms obtained from fitting the numerical simulation dataset, including both polynomial and power-type expressions. In general, the crater and energy metrics are expressed as either a polynomial form

$$Y = \alpha_0 + \alpha_1 W + \alpha_2 W^2 \tag{24}$$

or a power-law form

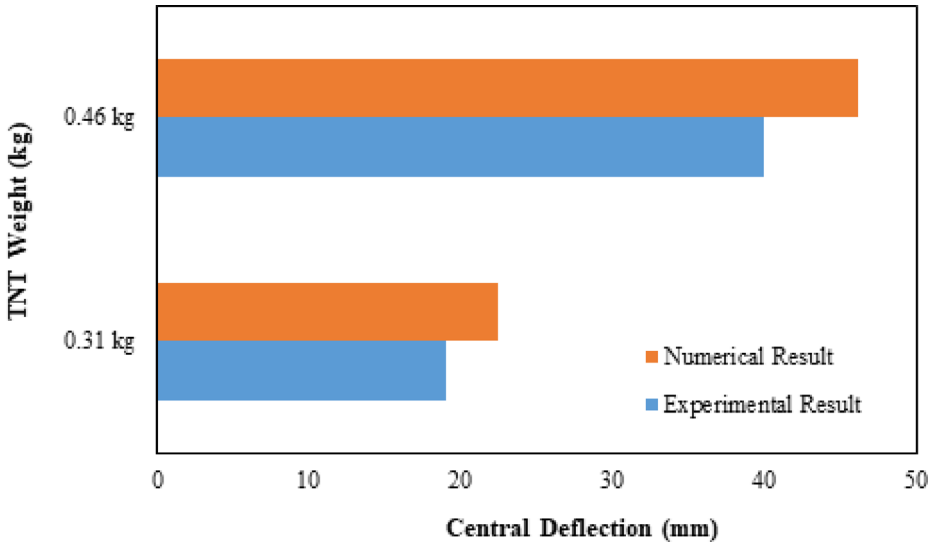

Fig. 13. Experimental and numerical comparison of deflection at the center of the RC slab.

$$Y = \beta W^n \tag{25}$$

where Y denotes the response quantity (e.g., crater diameter D_N(m), apparent depth H_N(m), or maximum energies KE, PDE, SE (kJ)), and W is TNT charge mass (kg). The coefficients α_0, α_1, α_2, and β carry units chosen to ensure dimensional consistency (e.g., if Y is in kJ and W is in kg, then α_1 has units of kJ/kg, α_2 has units of kJ/kg^2, and β has units of kJ/kg^n). The exponent n is dimensionless and reflects the nonlinear scaling of the response with explosive charge.

These regressions are calibrated using simulations for $W = 25$–1000 kg TNT and are applicable to the studied configuration: sandy clay soil modeled using Mohr–Coulomb parameters listed in Tables 1 and 2, and a circular RC tunnel with 5 m internal diameter and 0.35 m lining thickness subjected to surface blast loading (CONWEP). Extrapolation beyond the calibrated charge range or to substantially different soil types, saturation states, constitutive models, tunnel geometries, or boundary conditions should be avoided without recalibration.

Recompute crater diameter (D) and apparent depth (H)

This section presents the empirical formulae for crater diameter (D) and apparent depth (H) (refer to Eqs. 22 and 23) as provided by Ambrosini et al.[23], which have been reformulated by numerical analysis for 40 different TNT weights (25 kg, 50 kg, 75 kg, …, 1000 kg). Figure 14a depicts crater formation in the soil by illustrating the relationship between horizontal distance and settlement for a specific TNT charge. Figure 14b presents the variation in crater diameter and apparent depth on the soil surface for different TNT weights (25 kg, 50 kg, 75 kg, …, 1000 kg). The primary axis of the graph represents the crater diameter, while the secondary axis denotes the apparent depth. Regression analysis has established a relationship between crater diameter (D_N) and apparent depth (H_N) about TNT weight, as demonstrated in Eqs. 26 and 27. The coefficient of determination (R^2) for the crater diameter and apparent depth equations is 0.992 and 0.982, respectively, following regression analysis.

To authenticate, compare these equations with those presented by Ambrosini et al.[23] by graphing the relationship between crater diameter and apparent depth with some selected TNT weight (100 kg, 200 kg, 300 kg, 400 kg,…0.1000 kg) as shown in Fig. 15a and b. The graph reveals that these equations closely align with the Ambrosini et al.[23] equations.

$$D_N = 0.446(w)^{0.329} \tag{26}$$

$$H_N = 0.154ln\,(w) - 0.346 \tag{27}$$

where D_N denotes the crater diameter as determined by numerical analysis in meters, H_N signifies the apparent depth as ascertained by numerical analysis in meters, and w represents the weight of the TNT in kg.

The settlement contour for 1000 kg has been shown in Fig. 16. Although the direct deformation in the soil has not been noticed to reach up to the crown of the tunnel, significant damage has been reported in the concrete liner, as discussed in Sect. "Effect of TNT weight".

Effect of TNT weight

The response of the soil-tunnel system has been analyzed for various TNT weights, with the present analysis considering charges up to 1000 kg. While a 1000 kg TNT surface blast is rare, it remains relevant in wartime scenarios. The kinetic energy (KE) released due to the blast reaches its peak at 0.0018 s, as shown in Fig. 17a for selected TNT weights. After 0.05 s, the residual KE values converge across different TNT weights. However, at peak time, the KE generated by a 1000 kg TNT blast is approximately 27 times greater than that of a 100 kg TNT

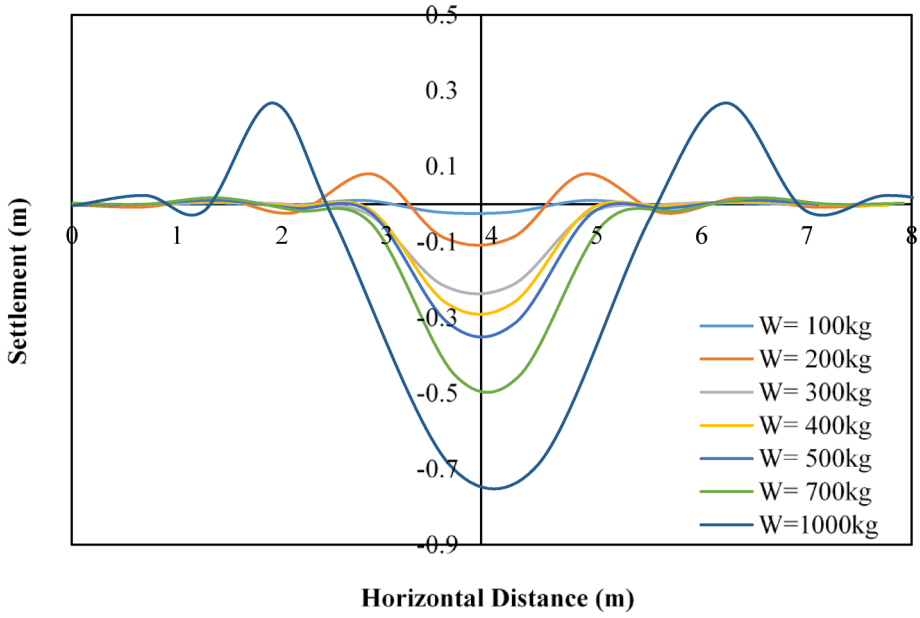

(a)

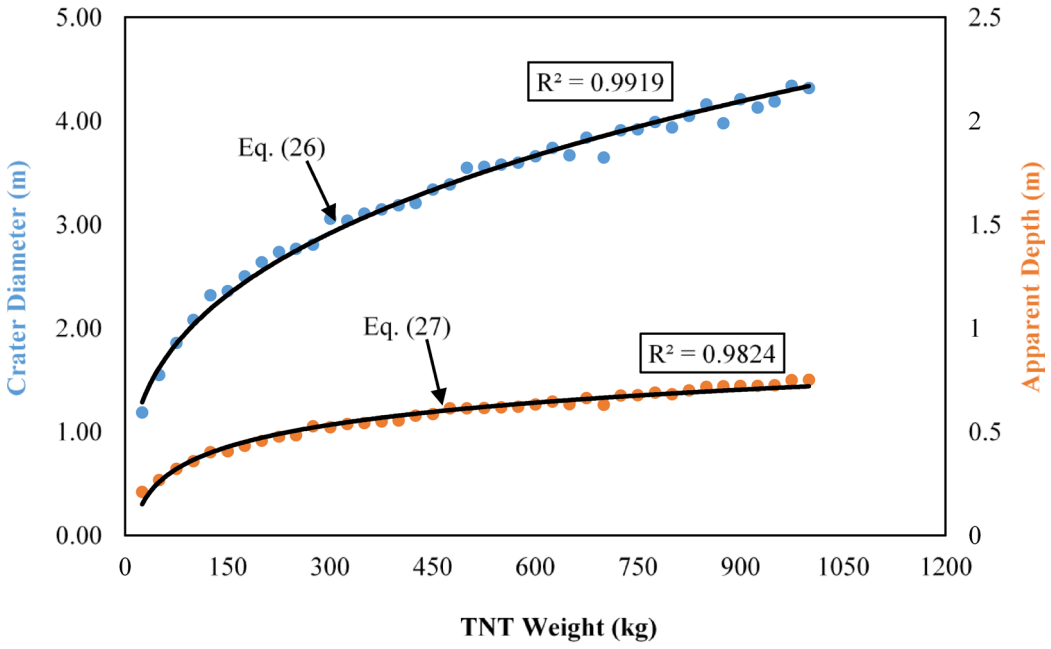

(b)

Fig. 14. (**a**) Settlement of soil for selected TNT charge weights (**b**) Variation of crater diameter and apparent depth with TNT charge weight (25–1000 kg).

explosion. Figure 17b illustrates the relation of maximum kinetic energy generated as a function of TNT weight (25 kg, 50 kg, 75 kg, …, 1000 kg). A relationship has been established between maximum KE and TNT weight through regression analysis with an R^2 value of 0.996. Equation 28 illustrates the correlation between TNT and maximum KE.

$$KE = 1.338(w)^{1.35} \tag{28}$$

where, KE Represents maximum kinetic energy in kilojoules (kJ) and w denotes the weight of the TNT in kilograms (kg).

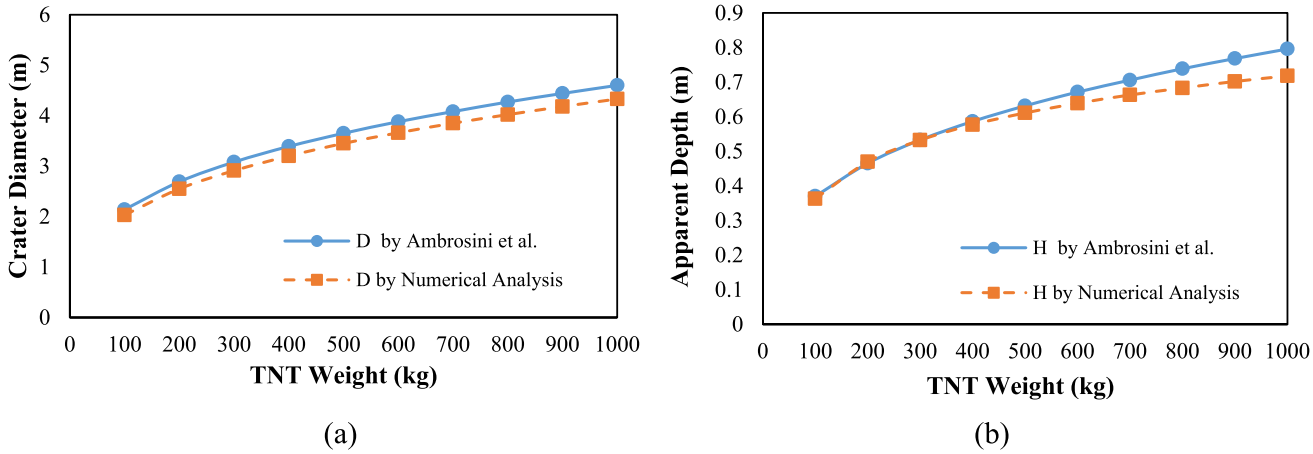

Fig. 15. Comparison of the numerical equation and Ambrosini et al.[23] equation (**a**) Crater diameter (**b**) Apparent depth.

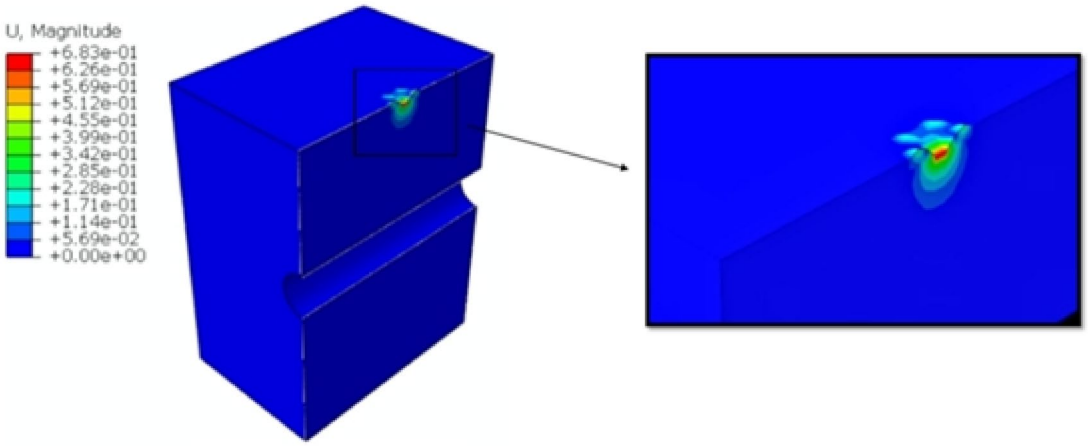

Fig. 16. The settlement in soil and crater formation due to the TNT weight of 1000 kg.

When a material undergoes a permanent alteration in shape or volume, even after unloading, some energy is irreversibly dissipated. Hence, plastic dissipation energy (PDE) is a measure of plastic failure induced in the material and the transfer of mechanical energy into thermal energy. Variation in the plastic dissipation energy in the time domain is shown in Fig. 18a. The permanent damage has been observed at approximately 0.045 s. However, a non-linear increase in deformation with an increase in TNT weight has been noted as shown in Fig. 18b, and the relation between PDE and TNT weight has been found as mentioned in Eq. 29.

$$PDE = 0.003(w)^2 + 7.967w - 600 \tag{29}$$

where, PDE denotes maximum plastic dissipation energy in kJ, and w signifies TNT weight in kg.

The potential energy stored in soil is termed “strain energy." In geotechnical engineering, the strain energy (SE) approach is a valuable tool for understanding and predicting the collapse of underground structures. It relates the deformation and failure of the surrounding soil or rock to the energy accumulated and dissipated under loading conditions. Strain Energy Density (SED), i.e., the localized energy per unit volume, indicates a likelihood of failure initiation. Under the current study, the maximum strain energy was generated at 0.007 s, as shown in Fig. 19a. However, the increase in SE is found to be non-linear concerning TNT weight; see Fig. 19b. Hence, 20 times increase in strain energy has been observed as the weight of explosives increases from 100 to 1000 kg. From the regression analysis of the data, a relationship between induced strain energy and the TNT weight has been mentioned in Eq. 30 with a coefficient of determination R^2 equal to 0.995.

$$SE = 0.001(w)^2 + 6.668w - 300 \tag{30}$$

where, SE denotes maximum strain dissipation energy in kJ, and w signifies TNT weight in kg.

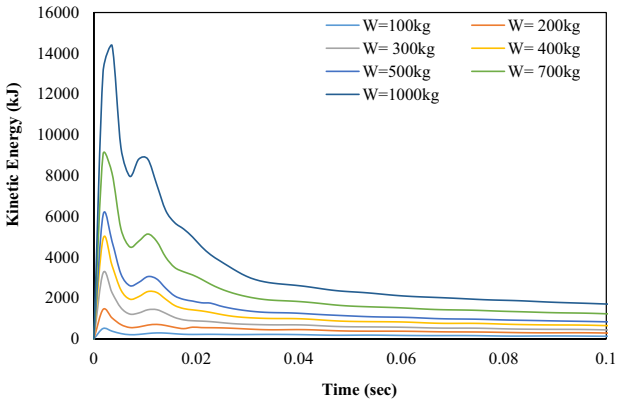

(a)

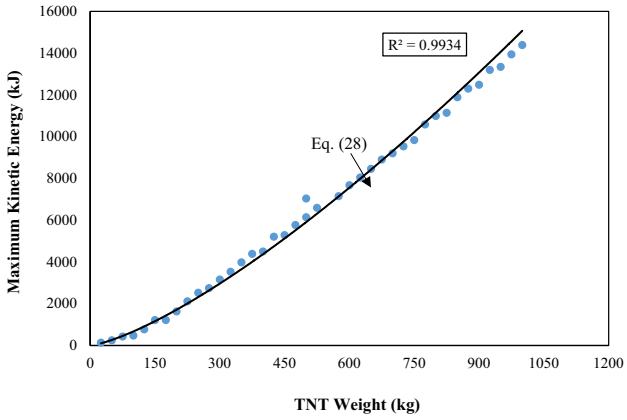

(b)

Fig. 17. (**a**) Time history of KE (kJ) generated in the surrounding sandy clay soil for selected TNT charge weights; (**b**) variation of maximum KE (kJ) with TNT charge weight (25–1000 kg).

The regression-based relationships between TNT charge weight and kinetic energy (KE), plastic dissipation energy (PDE), and strain energy (SE) quantify the transfer and dissipation of blast energy within the soil–tunnel system. The regression coefficients collectively reflect blast wave attenuation, soil plasticity, geometric confinement, and tunnel–soil interaction. KE represents inertia-driven stress-wave propagation, PDE corresponds to irreversible soil deformation and damage, and SE denotes recoverable elastic energy. The observed nonlinearity arises from the pressure-dependent mechanical response of sandy clay under increasing blast intensity.

These relationships are system-specific and applicable only within the investigated parameter range, including the adopted soil properties, tunnel geometry, and TNT charge weights (25–1000 kg). The regression coefficients are not universal and would require recalibration for different soil types, constitutive models, or tunnel configurations; thus, the proposed equations are intended for comparative and preliminary assessments rather than direct generalization.

The contours of stress induced in soil due to surface blasting are shown in Fig. 20; it may be very critical in the case of sandy clay. The gradient of stress is highly localized. Nevertheless, its effect was noticeable throughout the model. For a 500 kg weight, the peak Mises stress was 238 kPa, which increased to 432 kPa for a 1000 kg weight. It may be observed from the contour that the induced stresses were influencing the tunnel zone, which is 15 m below the detonation point. The damage induced in the tunnel liner has been discussed in the next section.

Assessment of safe depth

As an urban tunnel approaches the ground surface, its overburden depth progressively decreases, leading to increased vulnerability under surface blast loading. In this study, three representative soil–tunnel cross-sections with overburden depths of 15 m, 12 m, and 9 m were analyzed under varying TNT charge weights to quantitatively assess the concept of safe burial depth.

To move beyond a qualitative description, explicit performance-based criteria are introduced to define tunnel safety under blast loading. A burial depth is classified as safe if both of the following conditions are satisfied:

a. Tensile damage criterion: The maximum tensile damage index in the concrete lining remains below 0.30, corresponding to the initiation of microcracking without significant loss of structural integrity.

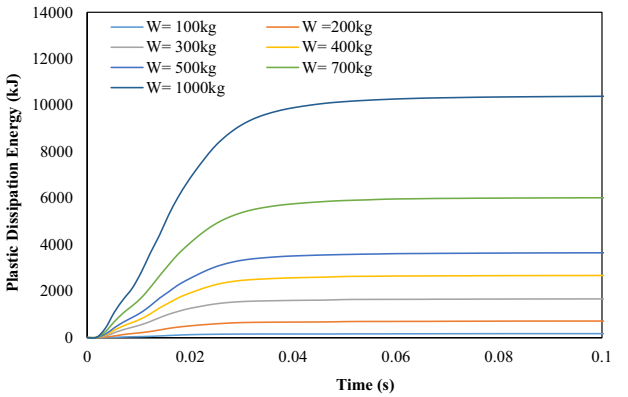

(a)

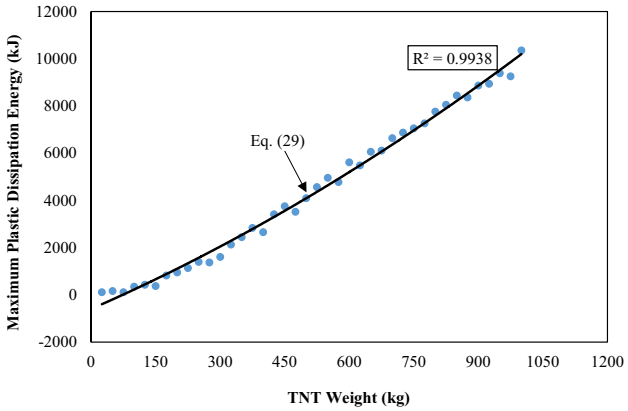

(b)

Fig. 18. (**a**) Time history of PDE (kJ) generated in the surrounding sandy clay soil for selected TNT charge weights; (**b**) variation of maximum PDE (kJ) with TNT charge weight (25–1000 kg).

b. Deformation criterion: The maximum tunnel liner deformation does not exceed 0.5% of the tunnel internal diameter, i.e.,

$$\delta/D \leq 0.005 \tag{31}$$

where δ is the maximum radial deformation and D is the tunnel internal diameter. This limit is commonly adopted as a serviceability threshold for circular underground structures subjected to extreme loading. Exceedance of either criterion is considered to indicate unsafe or potentially unacceptable performance.

Figure 21 and Table 5 present the maximum tunnel liner deformation as a function of TNT charge weight for the three overburden depths. The results demonstrate a clear depth dependency: for a given TNT weight, tunnel deformation consistently increases as burial depth decreases. As summarized in Table 5, reducing the overburden depth from 15 to 12 m results in a deformation increase of approximately 27–53%, while a reduction from 15 to 9 m leads to a substantially larger increase of approximately 57–97%, depending on TNT charge weight.

For example, under a 500 kg TNT surface blast, the maximum liner deformation increases from 27.65 mm at 15 m depth to 38.31 mm at 12 m depth and 48.79 mm at 9 m depth, corresponding to increases of 38.6% and 76.4%, respectively (Table 5). Similarly, for a 1000 kg TNT charge, deformation increases from 34.96 mm at 15 m depth to 54.98 mm at 9 m depth, representing an overall increase of 57.3%. These results indicate that, for most charge levels, a reduction in burial depth by one tunnel diameter leads to an increase in deformation on the order of 55–75%, with the amplification becoming more pronounced at lower TNT weights.

Since concrete is more vulnerable in tension than in compression, tensile damage is used as a primary indicator of structural failure. The tensile damage index ranges from 0.00 (undamaged) to 1.00 (complete failure). In post-processing, elements with damage values close to unity (0.99–1.00) were removed from visualization to indicate regions of total material failure. Figure 22 illustrates the tensile damage distribution for 500 kg and 1000 kg TNT charges.

Applying the defined safety criteria reveals that:

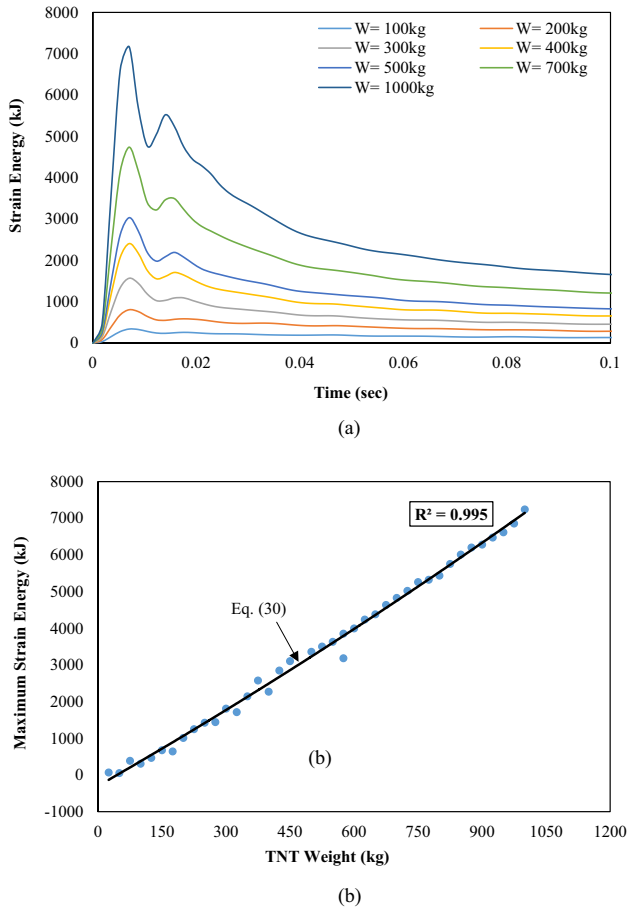

Fig. 19. (**a**) Time history of SE (kJ) generated in the surrounding sandy clay soil for selected TNT charge weights; (**b**) variation of maximum SE (kJ) with TNT charge weight (25–1000 kg).

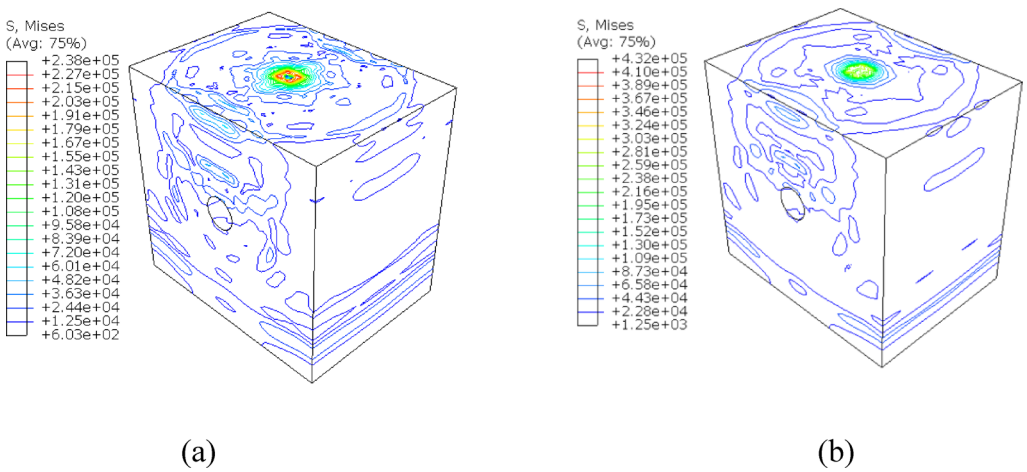

Fig. 20. The Stress in soil for different weights of TNT (**a**) 500 kg (**b**) 1000 kg.

- At an overburden depth of 15 m, tensile damage remains limited (damage index < 0.30) for TNT charges up to 500 kg, indicating safe performance. For a 1000 kg charge, localized regions exhibit damage indices approaching unity, suggesting the onset of unsafe behavior.
- At a depth of 12 m, both tensile damage and deformation criteria are exceeded for TNT charges greater than 500 kg, indicating marginal to unsafe performance.
- At a shallow depth of 9 m, extensive tensile damage (damage index ≈ 1.0) and excessive deformation occur for TNT charges exceeding 500 kg, clearly classifying this burial depth as unsafe under severe blast loading.

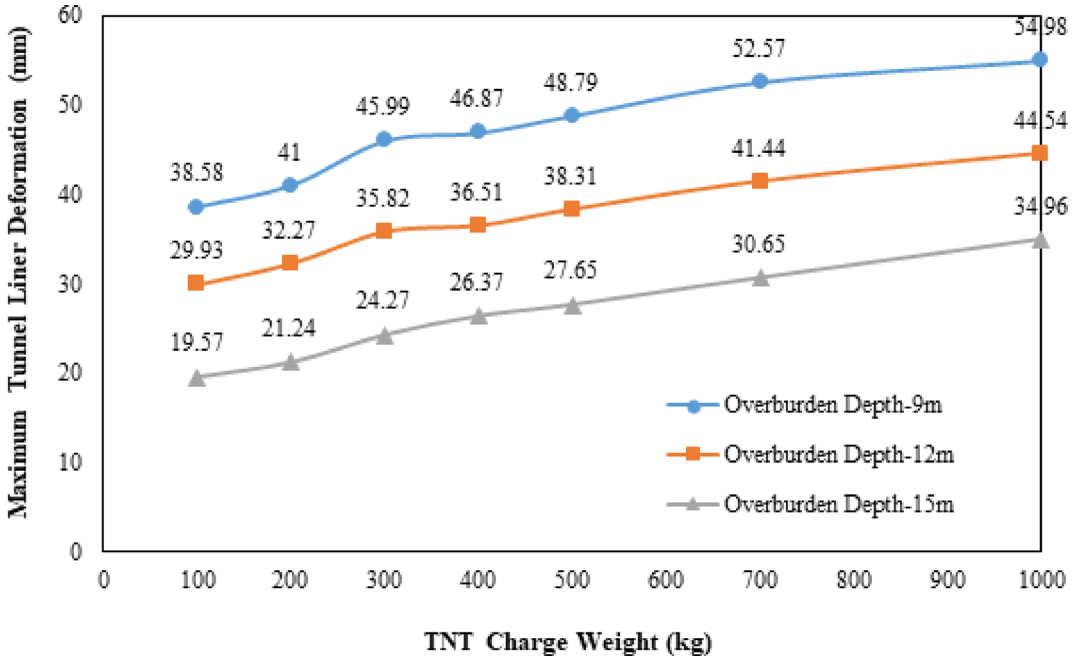

Fig. 21. Maximum deformation of the tunnel liner (mm) as a function of TNT charge weight for three overburden depths (9 m, 12 m, and 15 m).

TNT weight (kg)	Deformation at 15 m (mm)	Deformation at 12 m (mm)	Deformation at 9 m (mm)	Increase: 15→12 m (%)	Increase: 15→9 m (%)
100	19.57	29.93	38.58	53.0	97.1
200	21.24	32.27	41.00	51.9	93.1
300	24.27	35.82	45.99	47.6	89.5
400	26.37	36.51	46.87	38.5	77.7
500	27.65	38.31	48.79	38.6	76.4
700	30.65	41.44	52.57	35.2	71.6
1000	34.96	44.54	54.98	27.4	57.3

Table 5. Maximum tunnel liner deformation for different TNT charge weights and burial depths.

These results demonstrate that safe burial depth is strongly dependent on explosive charge magnitude and can be quantitatively identified using performance-based criteria. The proposed framework enables systematic classification of safe and unsafe burial depths and enhances the practical applicability of the results for rapid vulnerability assessment and comparative evaluation of underground tunnels subjected to surface blast loading.

Limitations and future work

It should be noted that the soil response is modeled using a simplified Mohr–Coulomb constitutive formulation, which represents an engineering approximation rather than a fully realistic description of high strain-rate soil behavior. Future studies incorporating rate-dependent and coupled hydro-mechanical soil models would further enhance the accuracy of absolute response predictions.

A systematic sensitivity study on domain size and boundary conditions, including non-reflecting or infinite elements, was not conducted in this work. Consequently, minor wave reflections from artificial boundaries may affect late-time stress oscillations in the soil domain. However, since key response metrics—such as peak tunnel deformation, tensile damage, and maximum energy components—occur during the early transient phase, the comparative trends and regression relationships are expected to remain robust. Future studies may incorporate absorbing boundaries and larger domains to further improve absolute response predictions.

Groundwater effects and pore-pressure generation were neglected in this study, although coupled hydro-mechanical behaviour under blast loading may significantly influence soil stiffness, wave propagation, and permanent deformation. Future work will incorporate solid–fluid interaction models to address these effects.

The tunnel lining was modelled as a continuous structure, neglecting segmental joints, interfaces, and interior components, which may affect local stiffness and damage patterns. These aspects will be considered in future tunnel-scale simulations. Only single-event surface blast loading was analysed. Since real tunnels may experience repeated or cumulative blasts, future studies will examine multi-blast scenarios to assess progressive damage and residual capacity.

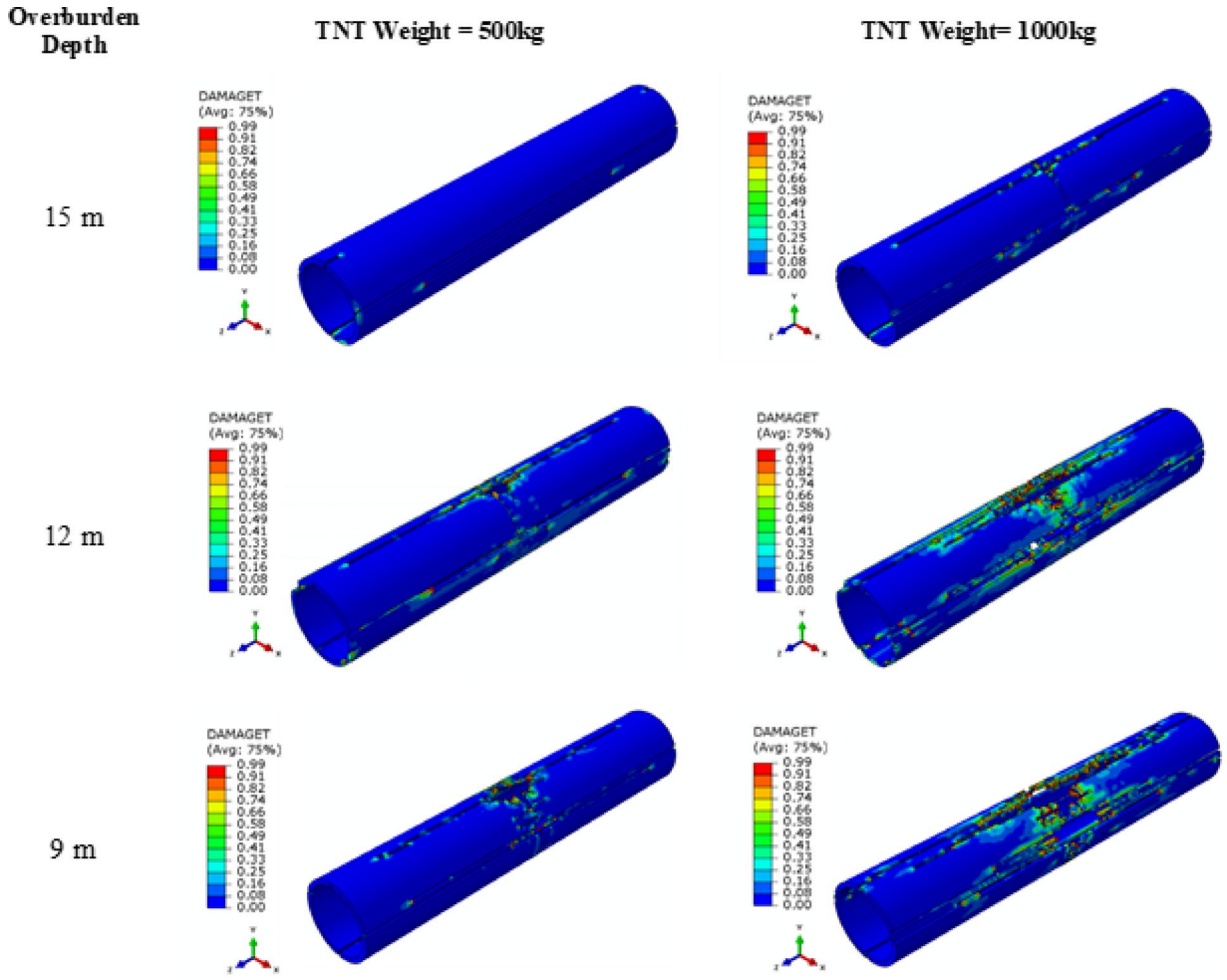

Fig. 22. Distribution of tensile damage in the tunnel liner for TNT charge weights of 500 kg and 1000 kg at overburden depths of 15 m, 12 m, and 9 m. Damage index values range from 0 (undamaged) to 1 (complete tensile failure).

Despite these limitations, the present study provides a consistent and quantitatively supported framework for evaluating soil–tunnel interaction under surface blast loading and establishes a basis for more advanced investigations.

Conclusions

A finite element simulation was conducted using Abaqus/Explicit to evaluate the dynamic response of soil–tunnel systems subjected to surface blasting. The CONWEP model, based on TM 5-855-1, was used to simulate surface blast loading within a 0.1-s window.

Key findings from the study are as follows:

1. The numerical model showed good agreement with empirical formulations and experimental data. Peak overpressures differed from TM 5–855-1 estimates by approximately 3–8%, while crater diameters exhibited a mean deviation of 4.3%. For reinforced concrete slab validation, peak displacement and damage predictions were within 10–15% of reported experimental results.
2. Blast-induced kinetic energy, plastic dissipation energy, and strain energy increased nonlinearly with TNT charge weight. Increasing the charge from 100 to 1000 kg resulted in an approximately 25–30-fold increase in kinetic energy and a 15–20-fold increase in plastic dissipation and strain energy, with regression fits yielding R^2 values greater than 0.99.
3. Tunnel liner deformation and tensile damage were strongly dependent on burial depth. Reducing the overburden from 15 to 9 m increased the maximum liner deformation by approximately 57–97%, depending on TNT charge weight, and led to extensive tensile cracking for charges exceeding 500 kg.
4. By introducing explicit performance criteria based on tensile damage index (< 0.3) and deformation-to-diameter ratio ($\delta/D \leq 0.005$), the concept of safe burial depth was quantitatively defined. An overburden depth of approximately 15 m was found to be safe for TNT charges up to 500 kg, whereas shallower depths exhibited unsafe performance under higher blast intensities.

5. The proposed regression-based energy and deformation relationships provide simplified tools for preliminary assessment, rapid vulnerability screening, and comparative evaluation of metro tunnels embedded in sandy clay deposits under surface blast loading. More detailed site-specific analyses remain necessary for final verification in critical infrastructure applications.

Data availability

The data supporting the findings of this study are available from the corresponding author upon reasonable request.

Received: 23 October 2025; Accepted: 24 February 2026
Published online: 09 March 2026

References

1. Tang, J., He, M., Bian, H. & Qiao, Y. Analytical solution for longitudinal seismic responses of circular tunnel crossing fault zone. *Int. J. Numer. Anal. Methods Geomech.* **48**(17), 4154–4177. https://doi.org/10.1002/nag.3841 (2024).
2. Roohezamin, A., Kalatehjari, R., Hajihassani, M., Kharghani, M. & Dias, D. Investigation of acoustic waves behavior of an underground tunnel in a multilayer soil. *Sci. Rep.* **12**(1), 13399. https://doi.org/10.1038/s41598-022-16991-w (2022).
3. Alsabhan, A. H. et al. Impact of large tunnel construction on existing small tunnels in soft ground: A multimethod analysis. *Adv. Civ. Eng.* **2025**(1), 1464028. https://doi.org/10.1155/adce/1464028 (2025).
4. Shitu, A., Shitu, E. & Rais, I. Deformation behavior of cross-passage tunnel in weak soils: A parametric study based on advanced soil models. *Transp. Infrastruct. Geotech.* **12**(7), 219. https://doi.org/10.1007/s40515-025-00679-5 (2025).
5. Richemond-Barak, D. *Underground warfare* (Oxford University Press, 2017).
6. Terrorism, Our world in data, https://ourworldindata.org/terrorism. (2021).
7. Jian, B. et al. Damage and reliability analysis of double-arch tunnel without a middle pilot tunnel under blast load. *Sci. Rep.* **14**(1), 9246. https://doi.org/10.1038/s41598-024-59681-5 (2024).
8. Higgins, W., Chakraborty, T. & Basu, D. A high strain-rate constitutive model for sand and its application in finite-element analysis of tunnels subjected to blast. *Int. J. Numer. Anal. Methods Geomech.* **37**(15), 2590–2610. https://doi.org/10.1002/nag.2153 (2013).
9. Rais, I., Ansari, M. A., Sadique, M. R., & Ansari, M. M. Effect of surface blast on soil and bunker liner with different curvature. In *International Conference on Advances in Concrete, Structural, & Geotechnical Engineering* (pp. 77–96). Springer Nature Singapore. https://doi.org/10.1007/978-981-96-0755-6_8 (2024).
10. Rais, I. et al. Finite element modelling and analysis of sustainable safety bunkers in war zones. *Sustain. Resilient Infrastruct.* https://doi.org/10.1080/23789689.2025.2496054 (2025).
11. Yu, L., Su, H., Jing, H., Zhang, Q. & Yang, E. Experimental study of the mechanical behavior of sandstone affected by blasting. *Int. J. Rock Mech. Min. Sci.* **93**, 234–241. https://doi.org/10.1016/j.ijrmms.2017.02.002 (2017).
12. He, C., Yang, J. & Yu, Q. Laboratory study on the dynamic response of rock under blast loading with active confining pressure. *Int. J. Rock Mech. Min. Sci.* **102**, 101–108. https://doi.org/10.1016/j.ijrmms.2018.01.011 (2018).
13. He, C. & Yang, J. Experimental and numerical investigations of dynamic failure process in rock under blast loading. *Tunn. Undergr. Space Technol.* **83**, 552–564. https://doi.org/10.1016/j.tust.2018.08.047 (2019).
14. De, A., Morgante, A. N., & Zimmie, T. F. Mitigation of blast effects on underground structure using compressible porous foam barriers. In *Poromechanics V: Proceedings of the Fifth Biot Conference on Poromechanics* (pp. 971–980). https://doi.org/10.1061/9780784412992.116 (2013).
15. Mobaraki, B. & Vaghefi, M. Numerical study of the depth and cross-sectional shape of tunnel under surface explosion. *Tunn. Undergr. Space Technol.* **47**, 114–122. https://doi.org/10.1016/j.tust.2015.01.003 (2015).
16. Mussa, M. H. et al. Assessment of damage to an underground box tunnel by a surface explosion. *Tunn. Undergr. Space Technol.* **66**, 64–76. https://doi.org/10.1016/j.tust.2017.04.001 (2017).
17. Mandal, J., Goel, M. D. & Agarwal, A. K. Dynamic response of underground tunnel in soft soil under surface and subsurface explosion. *Pract. Period. Struct. Des. Constr.* **27**(2), 04021081. https://doi.org/10.1061/(ASCE)SC.1943-5576.0000663 (2022).
18. Rashiddel, A., Kharghani, M., Dias, D. & Hajihassani, M. Numerical study of the segmental tunnel lining behavior under a surface explosion–Impact of the longitudinal joints shape. *Comput. Geotech.* **128**, 103822. https://doi.org/10.1016/j.compgeo.2020.103822 (2020).
19. Hyde, D. W. Microcomputer programs CONWEP and FUNPRO, applications of TM 5-855-1,'fundamentals of protective design for conventional weapons'(User's Guide) (No. WESIRSL881) (1988).
20. Ansari, M. A., Rais, I., Sadique, M. R. & Samanta, M. Numerical analysis of cut-and-cover tunnels under surface blast loads and mitigation strategies. *Transp. Infrastruct. Geotechnol.* **12**(3), 1–37. https://doi.org/10.1007/s40515-025-00555-2 (2025).
21. Alsabhan, A. H., Ansari, M. A., Rais, I., Sadique, M. R., Alam, S., & Hamid, W. Numerical failure analysis of cut and cover tunnel against surface blast. In *Proceedings of the World Congress on Civil, Structural, and Environmental Engineering*. https://doi.org/10.11159/icgre25.172 (2025).
22. Khan, J. A., Rais, I., Sadique, M. R. & Alam, M. M. Numerical analysis of underground tunnels in various soil types under surface blast loading: A parametric study on damage, settlement, and safe depth. *J. Build. Pathol. Rehabil.* **10**(1), 70. https://doi.org/10.1007/s41024-025-00579-8 (2025).
23. Ambrosini, R. D. & Luccioni, B. M. Craters produced by explosions on the soil surface. *J. Appl. Mech.* **73**(6), 890–900. https://doi.org/10.1115/1.2173283 (2006).
24. Tiwari, R., Chakraborty, T. & Matsagar, V. Dynamic analysis of tunnel in soil subjected to internal blast loading. *Geotech. Geol. Eng.* **35**(4), 1491–1512. https://doi.org/10.1007/s10706-017-0189-9 (2017).
25. Bhowmik, D., Baidya, D. K. & Dasgupta, S. P. A numerical and experimental study of hollow steel pile in layered soil subjected to lateral dynamic loading. *Soil Dyn. Earthq. Eng.* **53**, 119–129. https://doi.org/10.1016/j.soildyn.2013.06.011 (2013).
26. Bhowmik, D., Baidya, D. K. & Dasgupta, S. P. A numerical and experimental study of hollow steel pile in layered soil subjected to vertical dynamic loading. *Soil Dyn. Earthq. Eng.* **85**, 161–165. https://doi.org/10.1016/j.soildyn.2016.03.017 (2016).
27. Lubliner, J., Oliver, J., Oller, S. & Onate, E. A plastic-damage model for concrete. *Int. J. Solids Struct.* **25**(3), 299–326. https://doi.org/10.1016/0020-7683(89)90050-4 (1989).
28. Lee, J. & Fenves, G. L. Plastic-damage model for cyclic loading of concrete structures. *J. Eng. Mech.* **124**(8), 892–900. https://doi.org/10.1061/(ASCE)0733-9399(1998)124:8(892) (1998).
29. Hafezolghorani, M., Hejazi, F., Vaghei, R., Jaafar, M. S. B. & Karimzade, K. Simplified damage plasticity model for concrete. *Struct. Eng. Int.* **27**(1), 68–78. https://doi.org/10.2749/101686616X1081 (2017).
30. Johnson, G. R. A constitutive model and data for metals subjected to large strains, high strain rates and high temperatures. In *Proceedings of the 7th International Symposium on Ballistics*, The Hague, Netherlands (1983).
31. Goel, M. D., Matsagar, V. A. & Gupta, A. K. Dynamic response of stiffened plates under air blast. *Int. J. Prot. Struct.* **2**(1), 139–155. https://doi.org/10.1260/2041-4196.2.1.139 (2011).
32. Abaqus verification Manual. http://abaqusdocs.eait.uq.edu.au/v6.11/books/ver/default.htm?startat=ch03s09abv220.html

33. Kingery, C. N., Bulmash, G., & Muller, P. Blast loading on above ground barricaded munition storage magazines (No. ARBRLTR02557) (1984).
34. Kinney, G. F. & Graham, K. J. *Explosive shocks in air* (Springer, Berlin, 2013).
35. Wang, W., Zhang, D., Lu, F., Wang, S. C. & Tang, F. Experimental study on scaling the explosion resistance of a one-way square reinforced concrete slab under a close-in blast loading. *Int. J. Impact Eng.* **49**, 158–164. https://doi.org/10.1016/j.ijimpeng.2012.03.010 (2012).

Acknowledgements
The authors would like to acknowledge the support provided by the Ongoing Research Funding program, (ORF-2026-473), King Saud University, Riyadh, Saudi Arabia.

Author contributions
Abdullah Alsabhan—formal analysis; funding,Junaid Ahmad Khan—software; writing—original draft, Ibraheem Rais- Data collection; software; writing orginal draft, Aklilu Shitu Gebremariam- data collection; software; writing; review & editing, Md. Rehan Sadique—conceptualization; supervision; writing—review & editing, Shamshad Alam—funding; supervision, Jibran Qadri—writing—review & editing; formal analysis.

Funding
No funding is available for this project.

Declarations

Competing interests
The authors declare no competing interests.

Additional information
Correspondence and requests for materials should be addressed to A.S.G.

Reprints and permissions information is available at www.nature.com/reprints.

Publisher's note Springer Nature remains neutral with regard to jurisdictional claims in published maps and institutional affiliations.